Geophys. J. Int. (2007) doi: 10.1111/j.1365-246X.2006.03285.x

Surface wave tomography of the Barents Sea and surrounding regions

Anatoli L. Levshin,[1] Johannes Schweitzer,[2] Christian Weidle,[3] Nikolai M. Shapiro[1,4] and Michael H. Ritzwoller[1]

[1] *Department of Physics, University of Colorado at Boulder, Boulder, CO* 80309*, USA. E-mail: levshin@tinker.colorado.edu*
[2] *NORSAR,* POB 53*,* NO-2027 *Kjeller, Norway*
[3] *Institutt for geofag, Universitetet i Oslo, Norway*
[4] *Institute de Physique du Globe, CNRS, Paris, France*

Accepted 2006 November 3. Received 2006 October 20; in original form 2006 April 18

SUMMARY

The goal of this study is to refine knowledge of the structure and tectonic history of the European Arctic using the combination of all available seismological surface wave data, including historical data that were not used before for this purpose. We demonstrate how the improved data coverage leads to better depth and spatial resolution of the seismological model and discovery of intriguing features of upper-mantle structure. To improve the surface wave data set in the European Arctic, we extensively searched for broad-band data from stations in the area from the beginning of the 1970s until 2005. We were able to retrieve surface wave observations from regional data archives in Norway, Finland, Denmark and Russia in addition to data from the data centres of IRIS and GEOFON. Rayleigh and Love wave group velocity measurements between 10 and 150 s period were combined with existing data provided by the University of Colorado at Boulder. This new data set was inverted for maps showing the 2-D group-velocity distribution of Love and Rayleigh waves for specific periods. Using Monte Carlo inversion, we constructed a new 3-D shear velocity model of the crust and upper mantle beneath the European Arctic which provides higher resolution and accuracy than previous models. A new crustal model of the Barents Sea and surrounding areas, published recently by a collaboration between the University of Oslo, NORSAR and the USGS, constrains the 3-D inversion of the surface wave data in the shallow lithosphere. The new 3-D model, BARMOD, reveals substantial variations in shear wave speeds in the upper mantle across the region with a nominal resolution of $1^\circ \times 1^\circ$. Of particular note are clarified images of the mantle expression of the continent-ocean transition in the Norwegian Sea and a deep, high wave speed lithospheric root beneath the Eastern Barents Sea, which presumably is the remnant of several Palaeozoic collisions.

Key words: crustal structure, European Arctic, lithosphere, surface waves, tomography, upper mantle.

1 INTRODUCTION

The goal of this study is to refine our knowledge of the structure and tectonic history of the European Arctic by combining all available seismological surface wave data, including historical data that were not used before for this purpose. This work should be considered in the context of on-going and planned developments in studying the Earth's polar regions, particularly during and following the International Polar Year of 2007–2008. We demonstrate how the improvement in data coverage leads to better depth and spatial resolution of the seismological model and the discovery of intriguing features of the upper mantle. The rapid growth of seismic observations in the Arctic in the coming years will provide further opportunities for extending and refining this model.

The structure of the crust and upper mantle beneath the European Arctic, and the Barents Sea especially, has been the subject of special interest among Earth scientists in the recent years (e.g. Vorren *et al.* 1990; Gudlaugsson *et al.* 1998; Breivik *et al.* 1999, 2002; Artyushkov 2004, 2005; Mann *et al.* 2004; Ebbing *et al.* 2005). This relatively small region includes a complex of diverse tectonic features such as the deep ocean, a continental margin, a mid-ocean ridge, an ancient shield, and a continental shelf with one of most prominent sedimentary basins in the world (Fig. 1a). The upper crust of the eastern Barents Sea shelf is relatively well studied, as this area is considered to have high oil and gas resources. The tectonic history of the basin, however, and its relation to the structure of the underlying mantle remains poorly understood. In addition, knowledge of the deep structure of this region is important for

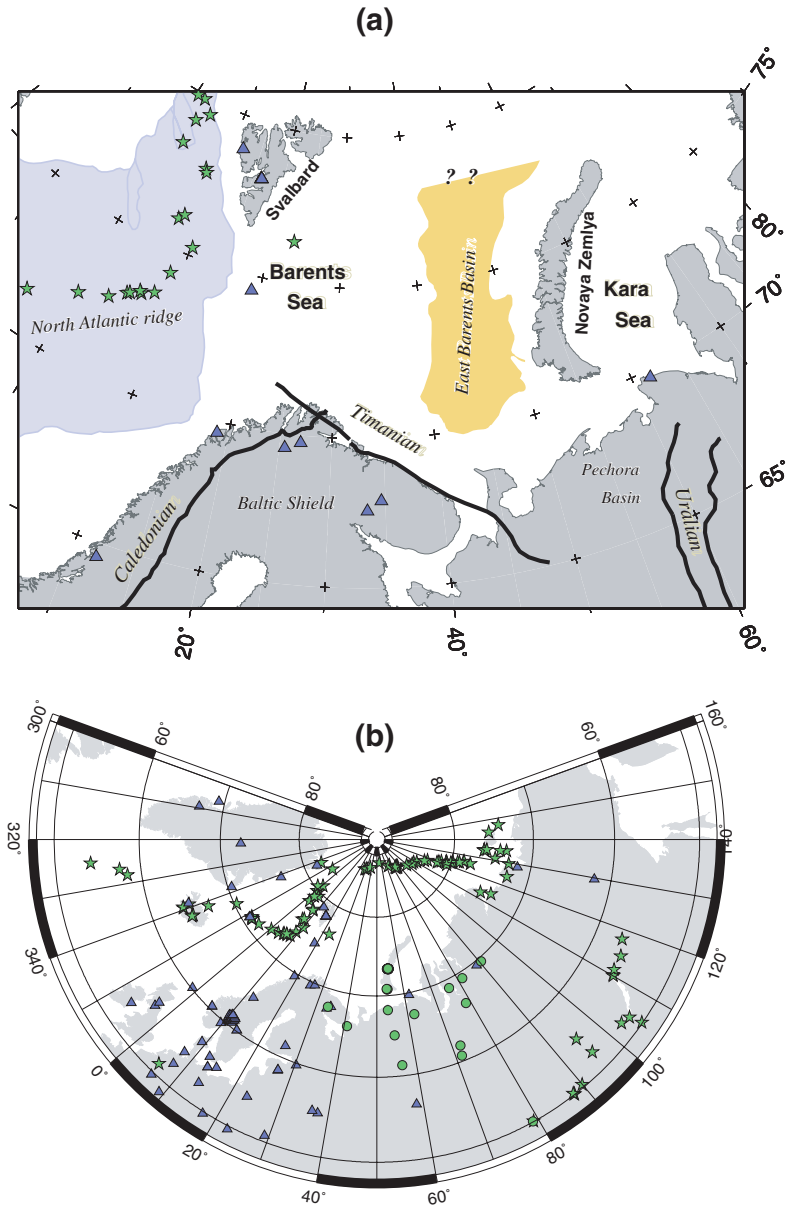

Figure 1. (a) The map shows the most relevant tectonic features discussed in the text. Blue shaded regions depict the north Atlantic oceanic domain, outlining the continent–ocean boundary in the European Arctic and the Norwegian Sea. The yellow shaded area in the East Barents Sea marks sediment thicknesses larger than 9 km in the East Barents Sea basin, after Johansen *et al.* (1992). Note that the geometry in the northern part of the basin is uncertain as indicated by question marks. The mid-Atlantic ridge is traced by the epicentres (green stars) and stations used in this study are displayed by blue triangles. (b) The map shows the location of the seismic stations (blue triangles) and events used in this study (see also Table 1). The epicentres of the earthquakes are shown by green stars, explosions as green circles.

monitoring seismic activity within the region, which includes the Soviet nuclear test site at Novaya Zemlya.

Kremenetskaya *et al.* (2001) published a 1-D velocity model for the wider Barents Sea region. Hicks *et al.* (2004) demonstrated that the 1-D model called *Barey* (Schweitzer & Kennett 2002, *cf.* Fig. 12), a slightly modified version of the Barents Sea model by Kremenetskaya *et al.* (2001) on top of model *ak135* (Kennett *et al.* 1995), is superior to other models for locating seismic events in the wider Barents Sea region. However, because of the known differences in the crustal structure, any 1-D model will have its limits in describing the velocity structure of the region.

The investigation of velocities in crust and uppermost mantle below the Barents Sea with surface waves started in 1970s. Calcagnile & Panza (1978) measured the interstation phase velocities of Rayleigh waves across the western part of the Barents Sea between stations KBS (Svalbard) and KRK (Norway) and inverted these measurements for an average crust and upper-mantle structure. McCowan *et al.* (1978) measured intersource phase velocities of Rayleigh waves from nuclear tests at two Soviet test sites at Novaya

Table 1. List of seismic stations from which surface wave data were retrieved to increase the ray coverage in the Barents Sea and surrounding regions (see also Fig. 1). The abbreviations in the network-affiliation column stand for: AWI—Alfred-Wegener-Institute for Polar and Marine Research, BGS—British Geological Service, CNSN—Canadian National Seismograph Network, FNSN—Finish National Network (University in Helsinki), FOI—Totalförsvarets forskningsinstitut (Sweden), GEUS—Danmarks og Grønlands Geologiske Undersøgelse, GRSN—German Regional Seismic Network, IDA—International Deployment of Accelerometers, IMS—International Monitoring System, IRIS—Incorporated Research Institutions for Seismology, KRSC—Kola Regional Seismological Center, MASI99—Temporal net of seismic stations in Finmark operated by NORSAR and the University of Potsdam (Germany) (Schweitzer 1999), NNSN—Norwegian National Seismic Network (University in Bergen), RUB—Ruhr University Bochum, UK—University in Kiel, and USGS—US Geological Survey. The data availability for some of the stations may be longer than known to us.

Station	Latitude	Longitude	Location	Network affiliation(s)	LP or BB data availability
AMD	69.7420	61.6550	Amderma	KRSC	08.1998–12.2003
APZ9	67.5686	33.4050	Apatity	KRSC	09.1992–
ARE0	69.5349	25.5058	ARCES Array	NORSAR/IMS	09.1987–
ARU	56.4302	58.5625	Arti	IRIS/IDA/IMS	09.1989–
BER	60.3870	5.3348	Bergen	NNSN	01.2004–
BILL	68.0651	166.4524	Bilibino	IRIS/USGS/IMS	08.1995–
BJO1	74.5023	18.9988	Bjørn Øya (Bear Island)	NNSN	06.1996–
BORG	64.7474	−21.3268	Borgarnes	IRIS/IDA	07.1994–
BSD	55.1139	14.9147	Bornholm	GEUS	01.1996–
COP	55.6853	12.4325	København	GEUS	09.1999–
DAG	76.7713	−18.6550	Danmarkshavn	GEUS/GEOFON/AWI	06 1998–
DSB	53.2452	−6.3762	Dublin	GEOFON	12.1993–
EDI	55.9233	−3.1861	Edinburgh	BGS	06.1996–
ESK	55.3167	−3.2050	Eskdalemuir	IRIS/IDA/BGS	09.1978–
FIA1	61.4444	26.0793	FINES Array	FNSN/IMS	04.2001–
HFC2	60.1335	13.6945	Hagfors Array	FOI/IMS	08.2001–
HFSC2	60.1326	13.6958	Hagfors Array (closed)	FOI	01.1992 –09.2003
HLG	54.1847	7.8839	Helgoland	UK/GEOFON	12.2001–
IBBN	52.3072	7.7566	Ibbenbüren	RUB/GEOFON/GRSN	07.1999–
JMI	70.9283	−8.7308	Jan Mayen (closed)	NNSN	10.1994–04.2004
JMIC	70.9866	−8.5057	Jan Mayen	NORSAR/IMS	10.2003–
KBS	78.9256	11.9417	Ny-Ålesund	NNSN/AWI/GEOFON/ IRIS/USGS	10.1986–09.1987 11.1994–
KEV	69.7553	27.0067	Kevo	FNSN/IRIS/USGS	10.1981–
KIEV	50.6944	29.2083	Kiev	IRIS/USGS	01.1995–
KONO	59.6491	9.5982	Kongsberg	NNSN/IRIS/USGS	09.1978–
KWP	49.6305	22.7078	Kalwaria Paclawska	GEOFON	06.1999–
LID	54.5481	13.3664	Liddow	GRSN/GEOFON	01.1994–10.1995
LRW	60.1360	−1.1779	Lerwick	BGS	08.2003–
LVZ	67.8979	34.6514	Lovozero	IRIS/IDA	10.1992–
MA00	69.5346	25.5056	at ARCES A0	MASI99	08.1999–10.1999
MA01	69.3752	24.2122	Suosjavrre	MASI99	05.1999–10.1999
MA02	69.1875	25.7033	Kleppe	MASI99	05.1999–10.1999
MA03	70.0210	27.3962	Sirma	MASI99	05.1999–10.1999
MA04	69.7127	29.5058	Neiden	MASI99	05.1999–10.1999
MA05	69.4533	30.0391	Svanvik	MASI99	05.1999–08.1999
MA06	70.4813	25.0609	Russenes	MASI99	05.1999–10.1999
MA07	69.7050	23.8203	Sautso	MASI99	05.1999–10.1999
MA08	70.1278	23.3736	Leirbotn	MASI99	05.1999–10.1999
MA09	69.4566	21.5333	Reisadalen	MASI99	05.1999–10.1999
MA10	69.5875	23.5273	Suolovuobme	MASI99	05.1999–10.1999
MA11	68.6595	23.3219	Kivilompolo	MASI99	05.1999–10.1999
MA12	69.8349	25.0823	Skoganvarre	MASI99	05.1999–10.1999
MA13	70.3161	25.5155	Børselv	MASI99	05.1999–10.1999
MBC	76.2417	−119.3600	Mould Bay	CNSN/IMS	04.1994–
MHV	54.9595	37.7664	Michnevo	GEOFON	05.1995–
MOL	62.5699	7.5470	Molde	NNSN	11.2000–05.2001
MOR8	66.2852	14.7316	Mo i Rana	NNSN	05.2001–08.2002
MORC	49.7766	17.5428	Moravsky Beroun	GEOFON	11.1993–
MUD	56.4559	9.1733	Mønsted	GEUS	12.1999–
N1002	60.4438	10.3690	NORSAR Array	NORSAR	03.1971–09.1976
N1103	60.5911	10.1956	NORSAR Array	NORSAR	03.1971–09.1976
N1201	60.8008	10.0386	NORSAR Array	NORSAR	03.1971–09.1976
N1303	61.0281	9.9381	NORSAR Array	NORSAR	03.1971–09.1976
N1403	61.1527	10.3090	NORSAR Array	NORSAR	03.1971–09.1976

Table 1. (*Continued.*)

Station	Latitude	Longitude	Location	Network affiliation(s)	LP or BB data availability
NAO01	60.8442	10.8865	NORSAR Array	NORSAR/IMS	03.1971–
NB201	61.0495	11.2939	NORSAR Array	NORSAR/IMS	03.1971–
NB302	60.9158	11.3309	NORSAR Array	NORSAR	03.1971–09.1976
NB400	60.6738	11.1881	NORSAR Array	NORSAR	03.1971–09.1976
NB504	60.5961	10.7794	NORSAR Array	NORSAR	03.1971–09.1976
NB603	60.6986	10.4358	NORSAR Array	NORSAR	03.1971–09.1976
NB701	60.9415	10.5296	NORSAR Array	NORSAR	03.1971–09.1976
NBO00	61.0307	10.7774	NORSAR Array	NORSAR/IMS	03.1971–
NC204	61.2759	10.7629	NORSAR Array	NORSAR/IMS	03.1971–
NC303	61.2251	11.3690	NORSAR Array	NORSAR/IMS	03.1971–
NC405	61.1128	11.7153	NORSAR Array	NORSAR/IMS	03.1971–
NC503	60.9075	11.7981	NORSAR Array	NORSAR	03.1971–09.1976
NC602	60.7353	11.5414	NORSAR Array	NORSAR/IMS	03.1971–
NC701	60.4939	11.5137	NORSAR Array	NORSAR	03.1971–09.1976
NC800	60.4756	11.0868	NORSAR Array	NORSAR	03.1971–09.1976
NC902	60.4084	10.6872	NORSAR Array	NORSAR	03.1971–09.1976
NCO00	61.3374	10.5854	NORSAR Array	NORSAR	03.1971–09.1976
NOR	81.6000	−16.6833	Nord	GEUS/GEOFON	08.2002–
NRE0	60.7352	11.5414	NORES Array	NORSAR	10.1984–06.2002
NRIL	69.5049	88.4414	Norilsk	IRIS/IDA/IMS	12.1992 –
NSS	64.5307	11.9673	Namsos	NNSN	10.2001–
OBN	55.1138	36.5687	Obninsk	IRIS/IDA	09.1988–
PUL	59.7670	30.3170	Pulkovo	GEOFON	05.1995–
RGN	54.5477	13.3214	Rügen	GRSN/GEOFON	12.1995–
RUE	52.4759	13.7800	Rüdersdorf	GRSN/GEOFON	01.2000–
RUND	60.4135	5.3672	Rundemannen	NNSN	03.1997–03.2003
SCO	70.4830	−21.9500	Ittoqqortoormiit (Scoresbysund)	GEUS	05.1999–
STU	48.7719	9.1950	Stuttgart	GEOFON/GRSN	04.1994–
SUMG	72.5763	−38.4540	Summit Camp	GEOFON	06.2002–
SUW	54.0125	23.1808	Suwalki	GEOFON	11.1995–
TIXI	71.6490	128.8665	Tiksi	IRIS/USGS/IMS	08.1995–
TRO	69.6345	18.9077	Tromsø	NNSN	03.2003–
TRTE	58.3786	26.7205	Tartu	GEOFON	06.1996–04.2003
VSU	58.4620	26.7347	Vasula	GEOFON	04.2003–
WLF	49.6646	6.1526	Walferdange	GEOFON	03.1994–
YAK	62.0308	129.6812	Yakutsk	IRIS/USGS/IMS	09.1993–

Zemlya recorded by the ALPHA array in Alaska to get the structural model under Novaya Zemlya. After the NORSAR array had been installed in Southern Norway, Bungum & Capon (1974) and Levshin & Berteussen (1979) observed mutlipathing of Rayleigh waves due to major tectonic boundaries in and around the European Arctic. Levshin & Berteussen (1979) investigated in detail surface wave observations from nuclear explosions on Novaya Zemlya and were able to derive a mean velocity model for the Barents Sea part of the path between Novaya Zemlya and NORSAR based on group and phase velocity observations. Chan & Mitchell (1985) and Egorkin *et al.* (1988) obtained average crustal models along several profiles crossing the Barents Sea using analogue records of earthquakes from seismic stations KHE (Franz Josef Land), APA (Kola Peninsula), KBS, KEV (Finland) and digital NORSAR data.

A surface wave tomography has been published for the Arctic, which shows the large scale velocity features in the larger Barents Sea region (Levshin *et al.* 2001; Shapiro & Ritzwoller 2002). This tomography based on group-velocity measurements of Love and Rayleigh waves, which had been compiled globally over the years at the University of Colorado. Recently, Pasyanos (2005) published group-velocity maps for Eurasia and the European Arctic, which show very similar large scale features. He used the University of Colorado data set and extended it by his own surface wave observations. However, he could not achieve higher resolution in the European Arctic due to the lack of additional regional surface wave observations.

Thus, all published global and regional tomographic models have poor resolution in the European Arctic due to the small number of seismic stations, relatively low regional seismicity, and limited *a priori* knowledge of the crustal structure. During the past decade, several new seismic stations were permanently or temporarily installed in and around this region. Many of the data from these stations are not easily accessible via the international data centres but only by direct request to the network operators. We have systematically searched during this study for additional broad-band waveform data observed at seismic stations and arrays in the area of interest from the early 1970s until 2005 (Levshin *et al.* 2005a,b). These newly analysed surface wave data are combined with a subset of the data from the University of Colorado (CU-Boulder). The resulting data set of Love- and Rayleigh-wave observations, for waves traversing the wider Barents Sea area, has a much higher path density than achieved in previous studies and thereby a higher resolution of lateral heterogeneities in seismic velocities.

Table 2. List with source parameters of the seismic events newly investigated during this study for measuring the group velocities of surface waves. A map with the event locations is shown on Fig. 1. All nuclear explosions are marked as 'exp'.

Latitude	Longitude	Depth	Year	Month	Day	Time	mb	Ms	Comment
61.2870	56.4660	0.0	1971	3	23	06:59:56.000	5.6	–	exp
73.3870	55.1000	0.0	1971	9	27	05:59:55.200	6.4	5.2	exp
73.3360	55.0850	0.0	1972	8	28	05:59:56.500	6.3	4.7	exp
52.3240	95.3660	33.0	1972	8	31	14:03:16.300	5.5	4.9	
73.3020	55.1610	0.0	1973	9	12	06:59:54.300	6.8	5.0	exp
70.7560	53.8720	0.0	1973	9	27	06:59:58.000	6.0	4.9	exp
64.7710	−21.0450	13.0	1974	6	12	17:55:08.700	5.5	5.3	
68.9130	75.8990	0.0	1974	8	14	14:59:58.300	5.5	–	exp
73.3660	55.0940	0.0	1974	8	29	09:59:55.500	6.4	5.0	exp
67.2330	62.1190	0.0	1974	8	29	14:59:59.600	5.2	–	exp
70.8170	54.0630	0.0	1974	11	2	04:59:56.700	6.7	5.3	exp
73.3690	54.6410	0.0	1975	8	23	08:59:57.900	6.4	4.9	exp
70.8430	53.6900	0.0	1975	10	18	08:59:56.300	6.7	5.1	exp
73.3510	55.0780	0.0	1975	10	21	11:59:57.300	6.5	–	exp
73.4040	54.8170	0.0	1976	9	29	02:59:57.400	5.8	4.5	exp
69.5320	90.5830	0.0	1977	7	26	16:59:57.600	4.9	–	exp
73.3760	54.5810	0.0	1977	9	1	02:59:57.500	5.7	–	exp
73.3360	54.7920	0.0	1978	8	10	07:59:57.700	5.9	4.3	exp
73.3800	54.6690	0.0	1978	9	27	02:04:58.200	5.6	4.5	exp
50.0460	78.9830	0.0	1978	11	4	05:05:57.500	5.6	4.2	exp
50.0530	79.0650	0.0	1979	7	7	03:46:57.400	5.8	–	exp
73.3690	54.7080	0.0	1979	9	24	03:29:58.300	5.7	–	exp
60.6770	71.5010	0.0	1979	10	4	15:59:57.900	5.4	–	exp
73.3380	54.8070	0.0	1979	10	18	07:09:58.300	5.8	–	exp
71.1920	−8.0300	10.0	1979	11	20	17:36:01.200	5.6	5.4	
73.3530	54.9970	0.0	1980	10	11	07:09:57.000	5.8	3.8	exp
68.2050	53.6560	0.0	1981	5	25	04:59:57.300	5.5	–	exp
73.3170	54.8120	0.0	1981	10	1	12:14:56.800	5.9	3.8	exp
69.2060	81.6470	0.0	1982	9	4	17:59:58.400	5.2	3.5	
73.3920	54.5590	0.0	1982	10	11	07:14:58.200	5.6	3.6	exp
73.3830	54.9130	0.0	1983	8	18	16:09:58.600	5.9	4.2	exp
73.3480	54.4950	0.0	1983	9	25	13:09:57.700	5.8	–	exp
65.0250	55.1870	0.0	1984	8	11	18:59:57.800	5.3	–	
61.8760	72.0920	0.0	1984	8	25	18:59:58.600	5.4	–	
67.7740	33.6880	0.0	1984	8	27	05:59:57.000	4.5	–	exp
73.3700	54.9550	0.0	1984	10	25	06:29:57.700	5.9	4.7	exp
65.9700	40.8630	0.0	1985	7	18	21:14:57.400	5.0	–	exp
63.8500	−19.7280	8.0	1987	5	25	11:31:54.300	5.8	5.8	
82.2290	−17.5560	10.0	1987	7	11	06:15:51.000	5.5	5.0	
73.3390	54.6260	0.0	1987	8	2	01:59:59.800	5.8	3.4	exp
74.6550	130.9620	10.0	1988	1	1	14:36:09.500	5.1	4.6	
77.6010	125.4510	10.0	1988	3	21	23:31:21.600	6.0	6.0	
73.3640	54.4450	0.0	1988	5	7	22:49:58.100	5.6	3.8	exp
66.3160	78.5480	0.0	1988	8	22	16:19:58.200	5.3	–	exp
73.3870	54.9980	0.0	1988	12	4	05:19:53.000	5.9	4.6	exp
71.1340	−7.6340	10.0	1988	12	13	04:01:38.900	5.7	5.6	
50.1030	105.3600	36.0	1989	5	13	03:35:02.800	5.6	5.6	
71.4320	−4.3710	10.0	1989	6	9	12:19:35.700	5.6	5.4	
76.1180	134.5780	10.0	1989	8	5	06:55:50.900	5.3	5.0	
76.1660	134.3460	13.0	1989	8	5	10:49:23.300	4.6	–	
76.1750	134.2460	10.0	1989	9	26	00:18:50.000	4.5	–	
80.6380	121.7610	31.0	1989	10	3	23:09:53.800	5.2	4.9	
80.5880	122.1320	10.0	1989	11	17	04:05:18.500	5.1	5.3	
73.3250	134.9090	18.0	1990	3	13	00:32:59.100	5.5	4.9	
74.2250	8.8280	29.0	1990	5	27	21:49:35.400	5.5	5.7	
75.0920	113.0960	33.0	1990	6	9	18:24:34.200	5.0	5.1	
64.6550	−17.6170	10.0	1990	9	15	23:07:42.800	5.5	5.2	
73.3610	54.7070	0.0	1990	10	24	14:57:58.100	5.7	4.0	exp
79.8490	123.8840	10.0	1991	3	22	17:02:19.500	4.7	4.1	
84.4010	108.2490	27.0	1991	6	11	07:16:34.400	5.5	5.3	
51.1530	5.7980	21.0	1992	4	13	01:20:00.800	5.5	5.2	
81.2460	121.2700	32.0	1992	6	8	09:30:16.100	5.1	4.6	

Table 2. (*Continued.*)

Latitude	Longitude	Depth	Year	Month	Day	Time	mb	Ms	Comment
64.7800	−17.5940	10.0	1992	9	26	05:45:50.600	5.5	5.4	
86.9410	56.0730	10.0	1993	2	23	11:56:27.100	4.7	4.6	
64.5780	−17.4820	9.0	1994	5	5	05:14:49.700	5.7	5.2	
56.7610	117.9000	12.0	1994	8	21	15:55:59.200	5.8	5.8	
78.3020	2.3020	10.0	1995	3	9	07:04:22.100	5.1	4.4	
50.3720	89.9490	14.0	1995	6	22	01:01:19.000	5.5	5.2	
51.9610	103.0990	12.0	1995	6	29	23:02:28.200	5.6	5.5	
75.9840	6.9560	10.0	1995	10	4	09:17:30.200	5.1	4.9	
56.1000	114.4950	22.0	1995	11	13	08:43:14.500	5.9	5.6	
72.6440	3.4880	10.0	1995	12	8	07:41:12.700	5.2	5.2	
75.8200	134.6190	10.0	1996	6	22	16:47:12.910	5.6	5.5	
77.8600	7.5640	10.0	1996	8	20	00:11:00.340	5.3	5.0	
77.7460	7.8770	10.0	1997	2	6	14:41:51.750	5.3	–	
78.5100	125.5150	10.0	1997	4	16	08:42:27.550	4.8	4.3	
78.4450	125.8210	10.0	1997	4	19	15:26:33.480	5.7	5.0	
73.4170	7.9880	10.0	1997	10	6	21:13:10.380	5.0	–	
79.8880	1.8560	10.0	1998	3	21	16:33:11.000	5.9	6.1	
72.8260	129.5830	10.0	1998	8	23	09:59:02.970	4.5	–	
86.2830	75.6090	10.0	1998	10	18	22:09:19.160	5.2	4.6	
85.6410	86.1000	10.0	1999	2	1	04:52:40.810	5.1	4.7	
85.7340	84.4390	10.0	1999	2	1	09:56:35.020	5.1	5.2	
85.6050	85.8370	10.0	1999	2	1	11:55:15.070	4.5	–	
85.5710	87.1410	10.0	1999	2	1	11:56:00.800	5.1	5.5	
85.5730	87.0370	10.0	1999	2	19	19:10:00.540	5.1	5.0	
86.2780	73.3940	10.0	1999	2	22	08:02:11.170	5.2	4.8	
51.6040	104.8640	10.0	1999	2	25	18:58:29.400	5.9	5.5	
85.6860	86.0340	10.0	1999	3	1	17:46:46.340	5.0	5.0	
85.6920	84.7970	10.0	1999	3	13	01:26:33.540	5.3	5.1	
85.6340	86.8190	10.0	1999	3	21	15:24:07.840	5.4	5.1	
55.8960	110.2140	10.0	1999	3	21	16:16:02.200	5.5	5.7	
85.6820	85.7360	10.0	1999	3	28	21:32:29.650	4.4	–	
85.6440	86.2590	10.0	1999	3	28	21:33:44.090	5.0	5.1	
85.6480	86.5310	10.0	1999	4	1	10:47:53.010	5.1	5.1	
73.2150	6.6500	10.0	1999	4	13	02:09:22.270	5.0	4.7	
85.6720	84.8300	10.0	1999	4	26	13:20:07.620	5.2	4.9	
85.6320	86.1460	10.0	1999	5	18	20:20:16.060	5.1	5.3	
85.6050	86.5260	10.0	1999	5	26	23:56:32.670	5.1	4.6	
73.0170	5.1870	10.0	1999	6	7	16:10:33.630	5.3	5.4	
73.0770	5.4530	10.0	1999	6	7	16:35:46.700	5.2	5.3	
85.6040	83.7040	10.0	1999	6	11	23:54:52.000	5.1	4.5	
85.6770	85.7720	10.0	1999	6	18	19:47:25.180	5.3	4.8	
70.2800	−15.3510	10.0	1999	7	1	02:08:02.010	4.9	–	
85.7410	83.2640	10.0	1999	7	8	19:25:10.520	5.0	4.6	
72.2610	0.3960	10.0	1999	8	3	13:55:41.410	5.0	5.1	
67.8630	34.3790	10.0	1999	8	17	04:44:35.950	4.6	–	
79.2210	124.3970	10.0	1999	10	27	05:05:07.180	4.8	4.5	
55.8300	110.0290	10.0	1999	12	21	11:00:48.870	5.5	5.0	
80.6150	122.1300	10.0	1999	12	26	08:39:48.390	4.7	–	
80.5820	122.2510	10.0	1999	12	30	06:46:55.250	4.7	4.4	
79.8020	123.0760	10.0	2000	1	16	12:29:12.630	4.5	3.8	
75.2710	10.1950	10.0	2000	2	3	15:53:12.960	5.5	5.0	
79.8900	0.4380	10.0	2000	2	12	09:05:06.630	5.0	4.7	
71.1900	−8.2630	10.0	2000	5	21	19:58:47.410	5.3	5.6	
63.9660	−20.4870	10.0	2000	6	17	15:40:41.730	5.7	6.6	
63.9800	−20.7580	10.0	2000	6	21	00:51:46.880	6.1	6.6	
74.3330	146.9720	10.0	2000	7	10	04:17:36.830	4.6	3.9	
78.9680	124.4680	10.0	2000	9	16	17:45:17.820	4.6	–	
54.7070	94.9830	33.0	2000	10	27	08:08:53.540	5.6	5.3	
81.5320	120.2790	27.3	2000	12	31	01:45:03.240	5.1	4.5	
80.0380	122.7240	10.0	2001	4	8	02:59:03.880	4.5	–	
80.4640	120.0940	10.0	2001	5	1	23:44:57.170	4.5	–	
82.9330	117.5090	10.0	2001	5	30	15:19:04.350	4.7	–	
72.6750	124.0160	61.5	2001	6	8	04:59:05.250	4.7	–	

Table 2. (*Continued.*)

Latitude	Longitude	Depth	Year	Month	Day	Time	mb	Ms	Comment
79.5140	4.1880	10.0	2001	7	16	14:09:29.240	5.0	4.5	
80.8480	0.7680	10.0	2001	12	8	06:44:22.020	5.1	4.8	
85.8580	27.6810	10.0	2002	5	3	11:19:20.320	4.1	–	
86.0050	31.5950	10.0	2002	5	3	11:20:51.540	5.2	5.4	
85.9720	31.1490	10.0	2002	5	3	15:33:34.880	5.1	5.1	
86.2760	37.1770	10.0	2002	5	28	15:39:01.550	4.9	4.7	
75.6340	143.7460	10.0	2002	6	4	00:05:07.170	4.8	–	
84.0830	110.6900	10.0	2002	6	9	21:20:38.750	4.5	–	
83.1360	−6.0780	10.0	2002	9	11	04:50:32.860	5.2	5.2	
66.9380	−18.4560	10.0	2002	9	16	18:48:26.720	5.5	5.7	
58.3110	−31.9460	10.0	2002	10	7	20:03:54.580	4.9	5.5	
57.4490	−33.3440	10.0	2003	2	1	18:47:52.150	5.3	5.5	
71.1220	−7.5770	10.0	2003	6	19	12:59:24.410	5.6	5.0	
76.3720	23.2820	10.0	2003	7	4	07:16:44.720	5.7	5.1	
73.2730	6.4210	10.0	2003	8	30	01:04:42.340	5.0	4.8	
56.0620	111.2550	10.0	2003	9	16	11:24:52.220	5.2	5.7	
80.3140	−1.8280	10.0	2003	9	22	20:45:16.910	5.2	4.7	
50.0380	87.8130	16.0	2003	9	27	11:33:25.080	6.5	7.5	
50.0910	87.7650	10.0	2003	9	27	18:52:46.980	6.1	6.6	
50.2110	87.7210	10.0	2003	10	1	01:03:25.240	6.3	7.1	
79.1410	2.3290	10.0	2003	10	7	02:36:54.440	5.1	4.6	
74.0800	134.8210	10.0	2003	12	7	09:16:12.640	5.0	4.4	
84.4750	105.2150	10.0	2004	1	19	07:22:52.910	5.5	5.2	
71.0670	−7.7470	12.2	2004	4	14	23:07:39.940	5.8	5.6	
81.7290	119.2920	10.0	2004	6	24	22:12:37.160	4.7	–	
54.1310	−35.2590	10.0	2004	7	1	09:20:44.140	5.4	5.5	
73.8300	114.4820	10.0	2004	10	2	11:06:01.470	4.5	–	
83.2630	115.9400	10.0	2004	11	13	21:28:01.450	4.6	–	
76.1690	7.5280	10.0	2004	11	27	06:38:29.290	5.0	4.5	
84.9480	99.3100	10.0	2005	3	6	05:21:43.430	6.1	6.2	

2 DATA COLLECTION AND ANALYSIS

To improve the data coverage in the target region, we have extensively searched for long period and broad-band data from seismic stations and arrays in the European Arctic, including local networks and temporary array installments. We were able to retrieve surface waveform data and make surface wave dispersion observations on data from archives at NORSAR, University of Bergen, the Kola Science Center in Apatity, the Geological Survey of Denmark and the University of Helsinki, in addition to data retrievable from the international data centres at IRIS and GEOFON. The full list of stations is given in Table 1 and an overview map of the station locations is in Fig. 1(b). New Love- and Rayleigh-wave data were identified for more than 150 seismic events (including 25 nuclear tests at Novaya Zemlya and 13 so-called Peaceful Nuclear Explosions (PNEs) within the former Soviet Union) spanning a time period from 1971 to 2005. Fig. 1(b) shows the geographic distribution of these events and their source parameters are listed in Table 2. The PNE data have not been used previously for surface wave studies.

From the surface wave recordings, group velocities for Love and Rayleigh waves were measured in the period range between 10 and 150 s using the program package for frequency–time analysis developed at CU-Boulder (Ritzwoller & Levshin 1998). Following outlier rejection (as described in Ritzwoller & Levshin 1998), the new measurements were combined with the existing set of group velocity measurements provided by CU-Boulder (Levshin *et al.* 2001) that were completely inside the study region [50°–90°N, 60°W–160°E]. The entire data set, therefore, consists of paths within the same regional frame. We should notice that CU-Boulder database includes more than 10 000 paths crossing this cell at periods 25 s and longer. However, we decided to limit ourselves only by the paths inside the cell to give new and earlier data the equal weight. Otherwise, all uncertainties related to the long paths could be imprinted on the resulting detailed regional maps.

By analyzing event clusters (Ritzwoller & Levshin 1998), the rms of the group velocity measurements for the new data set in the considered period range is measured to be 0.010–0.015 km s^{-1} for Rayleigh waves and 0.015–0.025 km s^{-1} for Love waves.

Fig. 2 compares the number of newly analysed Love and Rayleigh wave measurements with the number in the pre-selected CU data set. The new data set increases the ray density in the study region significantly. In particular, for shorter periods the number of rays crossing the target area is increased by more than 200 per cent for Rayleigh waves and close to 200 per cent for Love waves. For longer periods (i.e. $T > 80$ s), the percentage of new data significantly drops because large seismic events, necessary to generate long period radiation, are rare in the study region. Fig. 3 illustrates how the new data set complements the CU data at periods of 25 and 40 s. Note that many gaps in the pre-selected CU data set are filled by the new data. Fig. 4 shows the path densities for the combined data set for a variety of periods for both Love and Rayleigh waves. Due to the inhomogeneous distribution of sources and stations the path density is higher in the western part of the studied region and smoothly degrades towards the east. Path density degrades as periods rise above 40 s.

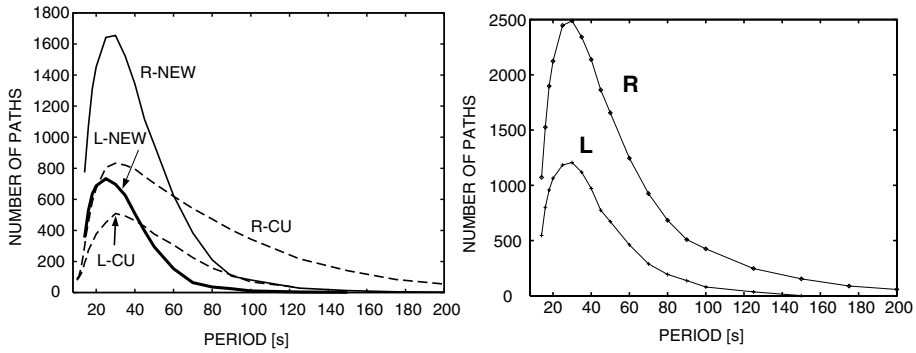

Figure 2. The figure on the left shows the number of observed ray paths, on which Love- (L) and Rayleigh-wave (R) group velocities were measured for the pre-selected CU-Boulder data set (dashed lines, R-CU and L-CU) and during this new study (solid lines, R-NEW and L-NEW). The figure on the right shows the total number of ray paths in the joint data set used for the inversions in this study.

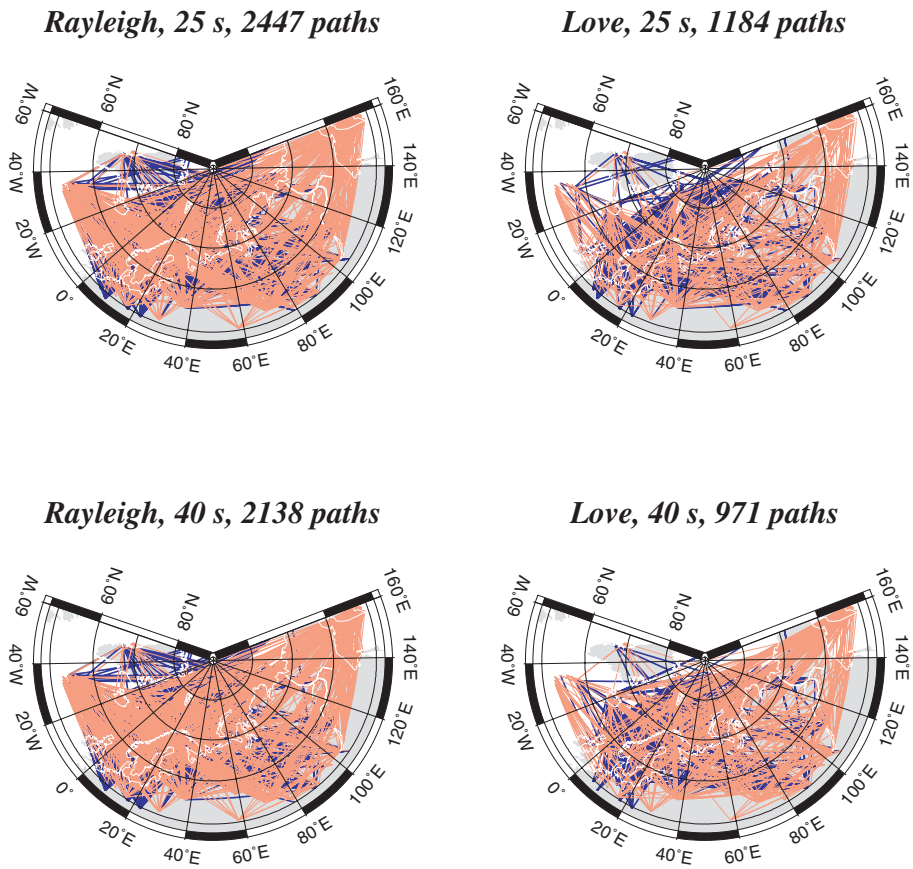

Figure 3. Path coverage for Rayleigh and Love waves at 25 and 40 s. Blue paths are the new data from this study and red paths represent data from the CU-Boulder data set. Note the gaps in the CU data set that are now covered through the new data.

3 2-D INVERSION FOR GROUP VELOCITY MAPS

A tomographic inversion for 2-D group-velocity maps has been performed for a set of periods between 14 and 90 s following the procedure described by Barmin *et al.* (2001) and Ritzwoller *et al.* (2002). In all cases, we inverted the combined data set of the newly acquired data and the pre-selected CU-Boulder data. As starting models for the inversion, the group-velocity maps predicted by the CUB2 global model (Shapiro & Ritzwoller 2002) were used. This model was constructed on $2^\circ \times 2^\circ$ grid using more than 200 000 group velocity measurements. We present the resulting group-velocity maps for Love (Fig. 5) and Rayleigh waves (Fig. 7) at four different periods: 18, 25, 40 and 60 s. The difference between the new group-velocity maps and the initial maps is also shown for Love (Fig. 6) and Rayleigh waves (Fig. 8).

The group-velocity maps show the lateral deviation of the group velocities from the average velocity in per cent. These deviations are up to 36 per cent for 16 s Love (Fig. 5) and Rayleigh waves (Fig. 7). This reflects the strong lateral heterogeneity of the Earth's crust in the region, which changes from the mid-oceanic ridge system in the North Atlantic to thick sedimentary basins in the

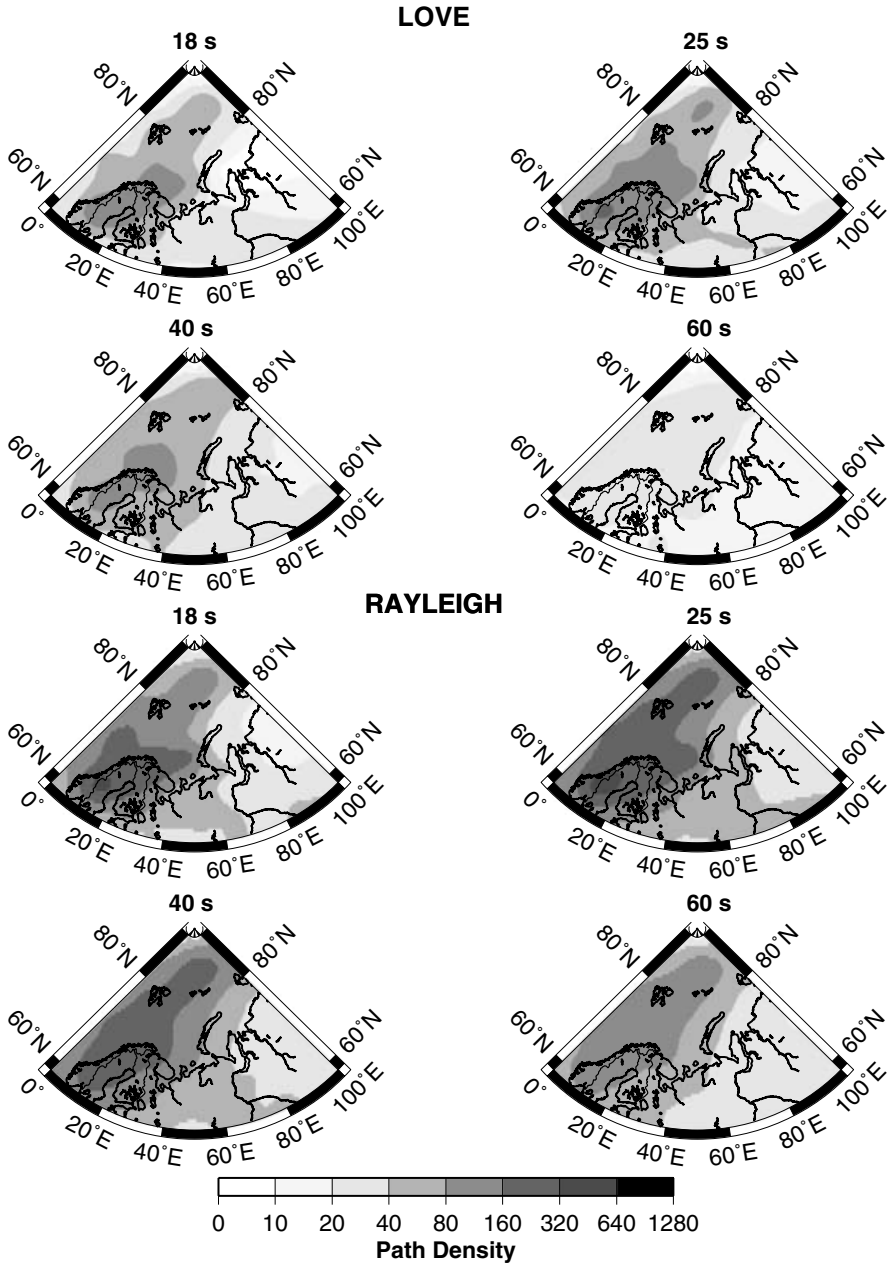

Figure 4. Path density maps for Love (top) and Rayleigh (bottom) waves for different investigated periods. Path density is defined as the number of paths crossing an equatorial $1^\circ \times 1^\circ$ cell.

Barents Sea and old shields with continental crust on mainland Fennoscandia. Comparison of the resulting and starting maps (Figs 6 and 8) demonstrates significant differences in velocities between the two sets of maps (up to 1.0–1.2 km s^{-1} for short periods and up to 0.25 km s^{-1} at period 60 s). This confirms the presence of new information in the new data set. Table 3 illustrates the improvement in the data fit achieved by the inversion. We compared the data fit achieved with selected data to that obtained with a combination of paths from the CU-B database crossing the studied region and new data (about 16 000 paths altogether for 40 s period). In the last case, the rms of the traveltime residuals is twice larger for the paths inside the region and the variance reduction for traveltimes residuals is only ∼10 and ∼9 per cent for group velocities. This could be expected as the initial model of Shapiro & Ritzwoller (2002) was built using the CU-B global data set. Including the same data for a new inversion does not add extra information. This comparison supports our decision to limit the data set to paths inside the studied area.

Because the sensitivity kernels for Love waves and Rayleigh waves are different, Rayleigh waves are sensitive for deeper structures than Love waves at the same period. Therefore, a joint analysis of the crustal structure with both Love and Rayleigh waves gives additional confirmation for an inverted velocity model. For example, note that the geographical pattern of group-velocity variations for Love waves at a period of 25 s (Fig. 5, top right) is similar to the pattern of group-velocity variations for Rayleigh waves at 18 s period (Fig. 7, top left). A similar relation can be found between the 40 s Love and the 25 s Rayleigh waves.

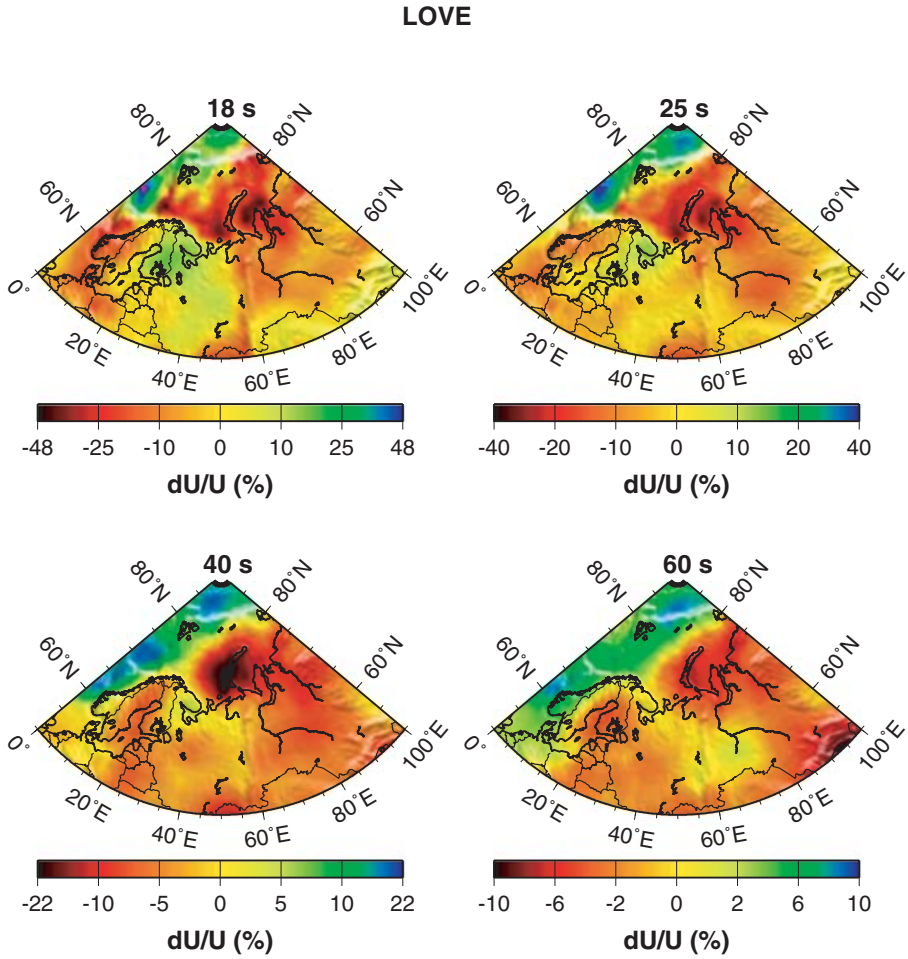

Figure 5. Results of the 2-D inversion for the group velocities of Love waves with period of 18, 25, 40 and 60 s. The maps present the 2-D distribution of the inverted group velocities as deviations from the average velocity across the region (in per cent).

To evaluate the spatial resolution of the estimated group velocity maps we used the technique described in Barmin *et al.* (2001). Fig. 9 illustrates the spatial resolution of the tomographic images for Rayleigh and Love waves at different periods. The best resolution (∼200 km) is observed for the Western Barents Sea and Southeastern Barents Shelf. Resolution degrades with increasing period above 40 s. The spatial resolution directly reflects the improvement in path coverage as shown in Figs 3 and 4.

4 INVERSION FOR A 3-D TOMOGRAPHIC VS MODEL

The 2-D group-velocity maps at periods up to 90 s derived from the new data set of Love and Rayleigh wave observations are the main input for a 3-D inversion for *S*-wave velocity structure. For longer periods (up to 200 s for Rayleigh waves and 150 s for Love waves) the CU-Boulder global group velocity and phase velocity maps were used as additional input data. Phase velocity data sets were provided by Harvard (Ekström *et al.* 1997) and Utrecht (Trampert & Woodhouse 1995) groups. Due to the small number of short period surface wave observations, however, the resolution is limited for details in the structure of the crust, particularly in the uppermost crust. In addition, shorter period surface waves are much more influenced by scattering at lateral heterogeneities in the crust. To improve the inversion with respect to that, we applied the new crustal model BARENTS50 of the Barents Sea and surrounding areas, which had been derived in a joint project by the University of Oslo, NORSAR, and the USGS (Bungum *et al.* 2005; Ritzmann *et al.* 2007). This model has detailed information on crustal thickness and sedimentary basins in the study region with a nominal resolution of 50 × 50 km and helps to constrain the tomographic inversion particularly in the shallow parts of the resulting inversion. We resampled the crustal model to a 1° × 1° grid and converted the *P*-wave velocities given by Ritzmann *et al.* (2007) to *S*-wave velocities applying the *P*-to-*S* velocity transformation as used in CRUST2.0 (Bassin *et al.* 2000; http://mahi.ucsd.edu/Gabi/rem.dir/crust/crust2.html). The upper crust of model BARENTS50 with its information on sedimentary coverage of the greater Barents Sea region was used as a constraint and not altered during the inversion. The parameters of the lower crust and the depth to the Mohorovičić discontinuity were initially taken from model BARENTS50, but allowed to change during the inversion. For the upper mantle part the CU-Boulder model of Shapiro & Ritzwoller (2002) was used as the initial model down to a depth of 250 km (see also http://ciei.colorado.edu/∼nshapiro/MODEL/index.html). Below 300 km, we applied the Harvard model J362D28 (Antolik *et al.* 2003) as input. A smooth transition was used between these two models in the depth range from 250 to 300 km.

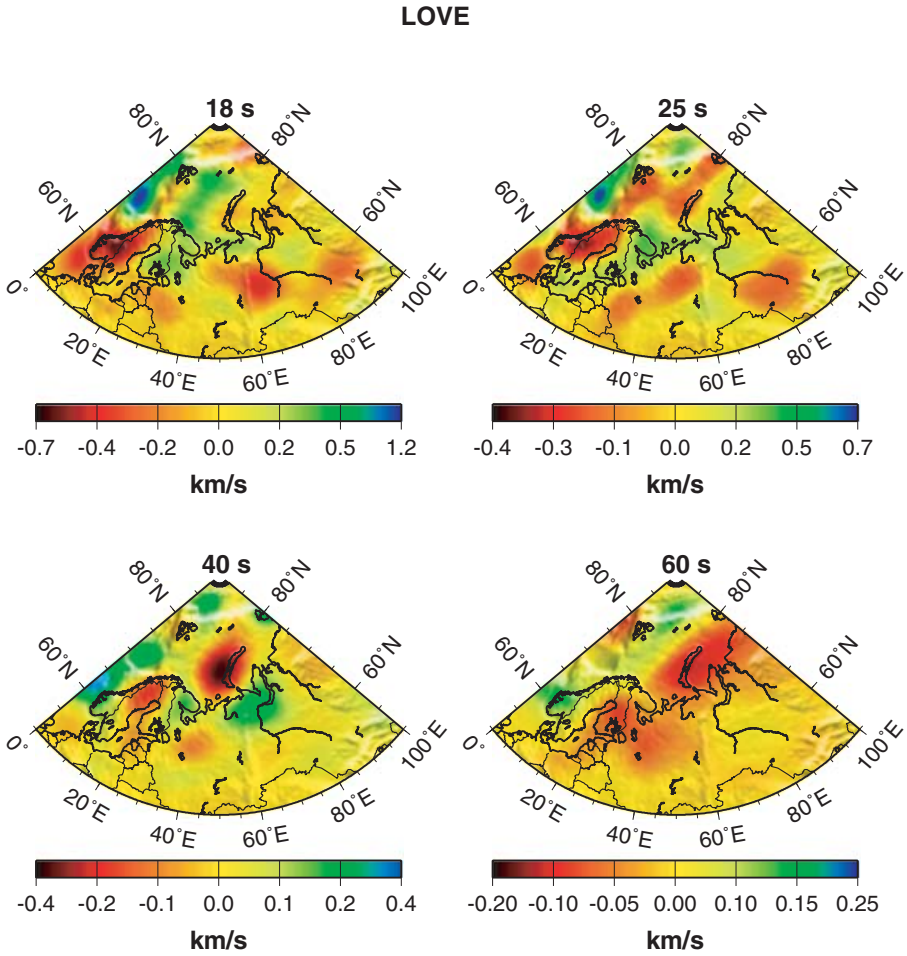

Figure 6. Difference between the initial and newly inverted group-velocity maps of Love waves with period of 18, 25, 40 and 60 s (in km s^{-1}).

The new 3-D shear velocity model is constructed using a Monte Carlo method, which is described in detail by Shapiro & Ritzwoller (2002). The inversion is performed at each node of a $1^\circ \times 1^\circ$ grid across the region of the study, and produces an ensemble of acceptable models that are constrained by a variety of *a priori* information, including the initial crustal model. Shapiro & Ritzwoller (2002) fully describe the set of constraints. The isotropic part of the model in the mantle is parametrized with B-splines. The model is radially anisotropic from the Moho to a variable depth that averages about 200 km. We will not discuss the anisotropic properties of the model but will concentrate only on the isotropic component of shear velocity $V_s = (V_{sv} + V_{sh})/2$ at all depths. Fig. 10 displays an example of the inversion at two points: one is in Barents Sea (74°N, 40°E), and the other in the Western Siberia (70°N, 70°E).

5 DISCUSSION OF THE 3-D VELOCITY MODEL BARMOD

The inversion results are presented as deviations in shear wave speed (in per cent) from the *S*-wave speed in the 1-D *Barey* model (Fig. 12, bottom). Fig. 11 shows several horizontal slices through the model in the range from 60 to 280 km depth. The horizontal slice for a depth of 45 km is shown in Fig. 12 relative to the 1-D reference model *Barey*. The shear velocity cross-sections along several transects across the studied region are shown in Fig. 13. The positions of these transects are plotted on the map in Fig. 12. The 3-D model BARMOD reveals lateral heterogeneities in shear wave speeds in the upper mantle across the whole region. Of particular interest are the imprints of first-order changes in the tectonic regimes, such as the mid-Atlantic ridge, the continent-ocean transition in the Norwegian Sea, and the thickened crust beneath Novaya Zemlya.

The structure of the lithosphere is naturally very closely related to its tectonic history. For the Barents Sea region, the evolution is characterized by repeated cycles of compression and extension making it a tectonically very complex system. Three stages of major convergence are known for the region related to the Timanian (600–545 Ma), Caledonian (440–410 Ma) and Uralian (280–240 Ma) orogenies (Faleide *et al.* 2006a,b). Since the last major tectonic activity in the region occurred some 240 Ma, we can assume that the high-velocity anomaly dipping eastward beneath Novaya Zemlya (Fig. 13) is not of thermal but of compositional origin. The timing of the active subduction is uncertain although there is evidence that it occurred as early as at the Timanian stage (Faleide, pers. comm.). Beneath the East Barents Sea basin, which evolved during late Permian—early Triassic times by rapid, non-fault-related subsidence (Gudlaugsson *et al.* 1998), the thickened mantle anomaly indicates a possible chronological relation of both processes (thickening in the mantle and subsidence in the crust), which in turn both correlate in time with the Uralian collision. The processes causing the thickening of the high-velocity anomaly can be both mechanical

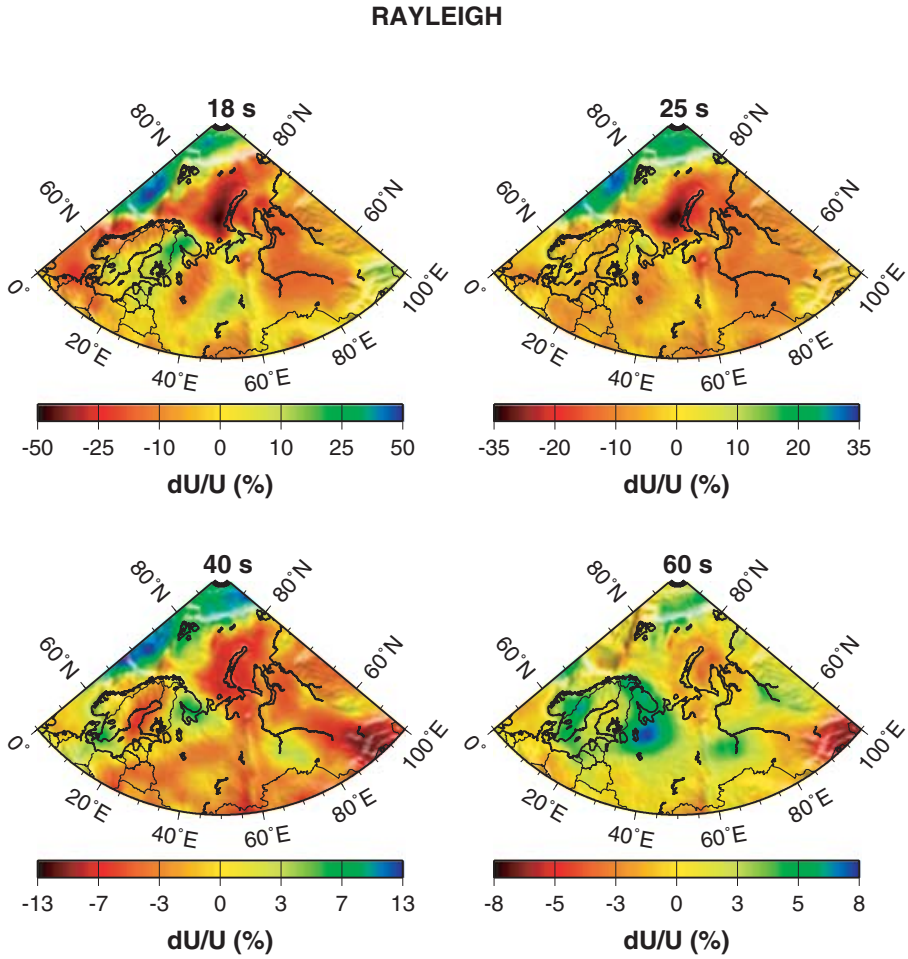

Figure 7. Results of the 2-D inversion for the group velocities of Rayleigh waves with period of 18, 25, 40 and 60 s. The maps present the 2-D distribution of the inverted group velocities as deviations from the average velocity (in per cent).

or compositional (phase changes) and the mechanisms linking the thickening in the upper mantle to basin formation are uncertain. The location of the Caledonian suture in the Barents Sea region is also uncertain, but Breivik *et al.* (2002) showed evidence that it may be situated in the western Barents Sea, approximately at the western boundary of the shallow upper mantle high-velocity anomaly. Thus, this western boundary could be related to lithosphere subducted during the Caledonian collision. For the Uralian collision, no clear onset of a subducting slab as an indicator for a suture location can be identified in the model.

The negative anomalies east and southeast of Svalbard at 140 km depth correlate nicely in geometry with an area influenced by major tectonic uplift (Dimakis *et al.* 1998). To the west, BARMOD clearly images the imprints of the mid-Atlantic ridge and the extension of a low-velocity anomaly beneath the continental lithosphere near the Svalbard Archipelago. In contrast to the high-velocity anomaly to the east, this low velocity anomaly probably is thermal in origin, related to break-up of the northeastern Mid-Atlantic during the Cenozoic. Faleide *et al.* (2006a) compared BARMOD with thermal modelling across the continent–ocean boundary (Breivik *et al.* 1999) revealing a clear correlation between the modelled isotherms and the velocity field.

The velocity variations at 45 km depth, presented in Fig. 12, reveal approximately the lateral change in *S*-wave velocity relevant for Sn propagation. Engdahl & Schweitzer (2004a,b) described pronounced differences in traveltimes and waveform shapes on NORSAR array recordings of nuclear explosions conducted both at the northern and at the southern nuclear test side on Novaya Zemlya. This observation may be explained by multipathing effects due to the dipping high velocity body.

6 CONCLUSIONS

The substantial data set of new surface wave group-velocity measurements combined with existing data from CU-Boulder has provided the opportunity for constructing a new 3-D shear velocity model of the crust and upper mantle down to about 250 km depth beneath the European Arctic. This 3-D Vs model, BARMOD, has higher spatial and depth resolution than previous models and clarifies or reveals important features of the tectonic setting in the region: continent-ocean boundary, a dipping slab-like high velocity zone in the upper mantle and the thermal extension of the northeastern Mid-Atlantic ridge system. The contemporaneous thickening of the high-velocity body beneath the eastern Barents Sea basin with crustal subsidence is an intriguing indicator for the presence of mechanic coupling between crustal and upper-mantle structure, the details of which are yet poorly understood.

Apart from providing *S*-wave velocities, BARMOD also contains *P*-wave velocities and densities which were derived by

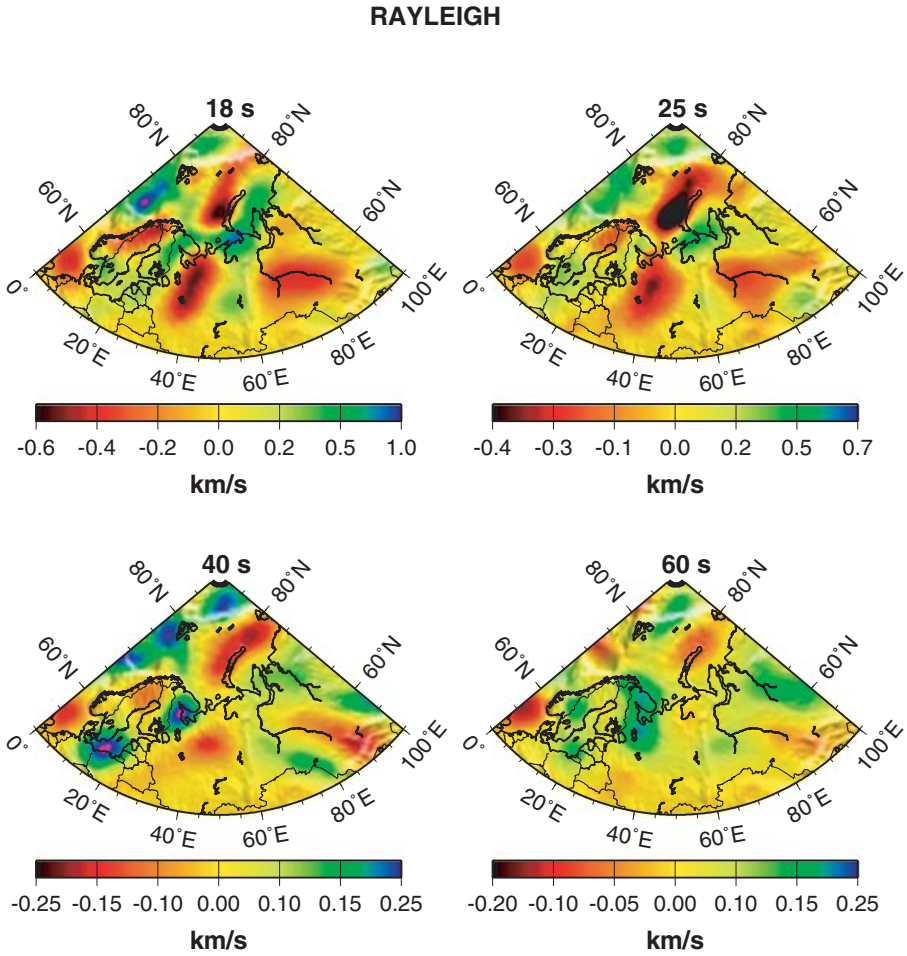

Figure 8. Difference between the initial and newly inverted group-velocity maps of Rayleigh waves with period of 18, 25, 40 and 60 s (in km s^{-1}).

Table 3. Statistics of the improvements in data fitting with the newly constructed group-velocity maps: Wave—wave type (Love/Rayleigh); T—period ; δt_0—starting rms of traveltime residuals predicted by the CU-Boulder model; δt—resulting rms of the traveltime residual; S_t – variance reduction of traveltime residuals; δU_0—starting rms of the group velocity residual; δU—resulting rms of the group-velocity residuals; S_U—variance reduction of the group velocity residuals.

Wave	T (s)	δt_0 (s)	δt (s)	S_t (per cent)	δU_0 (km s^{-1})	δU (km s^{-1})	S_U (per cent)
L	18	42.4	27.8	56.9	0.167	0.109	57.5
L	25	27.0	19.1	49,7	0.110	0.083	43.0
L	40	16.5	12.0	47.5	0.079	0.054	52.0
L	60	14.9	10.3	52.5	0.063	0.050	37.7
R	18	50.8	22.5	80.3	0.172	0.079	79.2
R	25	37.0	15.9	81.5	0.139	0.056	83.6
R	40	17.7	10.1	67.6	0.076	0.040	73.0
R	60	15.8	10.1	58.8	0.066	0.043	57.0

using temperature–velocity relations for mantle material as described in Goes *et al.* (2000) and Shapiro & Ritzwoller (2004). Among an undefined set of optional applications, this complete velocity and density model for the crust and upper most mantle of the wider Barents Sea region may be used for refining source specific traveltime corrections (SSSCs) for regional *P* and *S* waves propagating through the larger Barents Sea region as described in Ritzwoller *et al.* (2003). The new 3-D velocity model of the wider Barents Sea region can be downloaded from the web-page http://www.norsar.no/seismology/barents3d/.

ACKNOWLEDGMENTS

For this study, we requested and retrieved broad-band and long- period data from the Norwegian National Seismic Network (NNSN, University in Bergen), Kola Regional Seismological Center (KRSC, Apatity), Danmarks og Grønlands Geologiske Undersøgelse (GEUS, Copenhagen), Totalfårsvarets forskningsinstitut (FOI, Stockholm), British Geological Service (BGS, Edinburgh), the Finish National Seismic Network (FNSN, University of Helsinki), the international networks (GSN and GEOFON) and

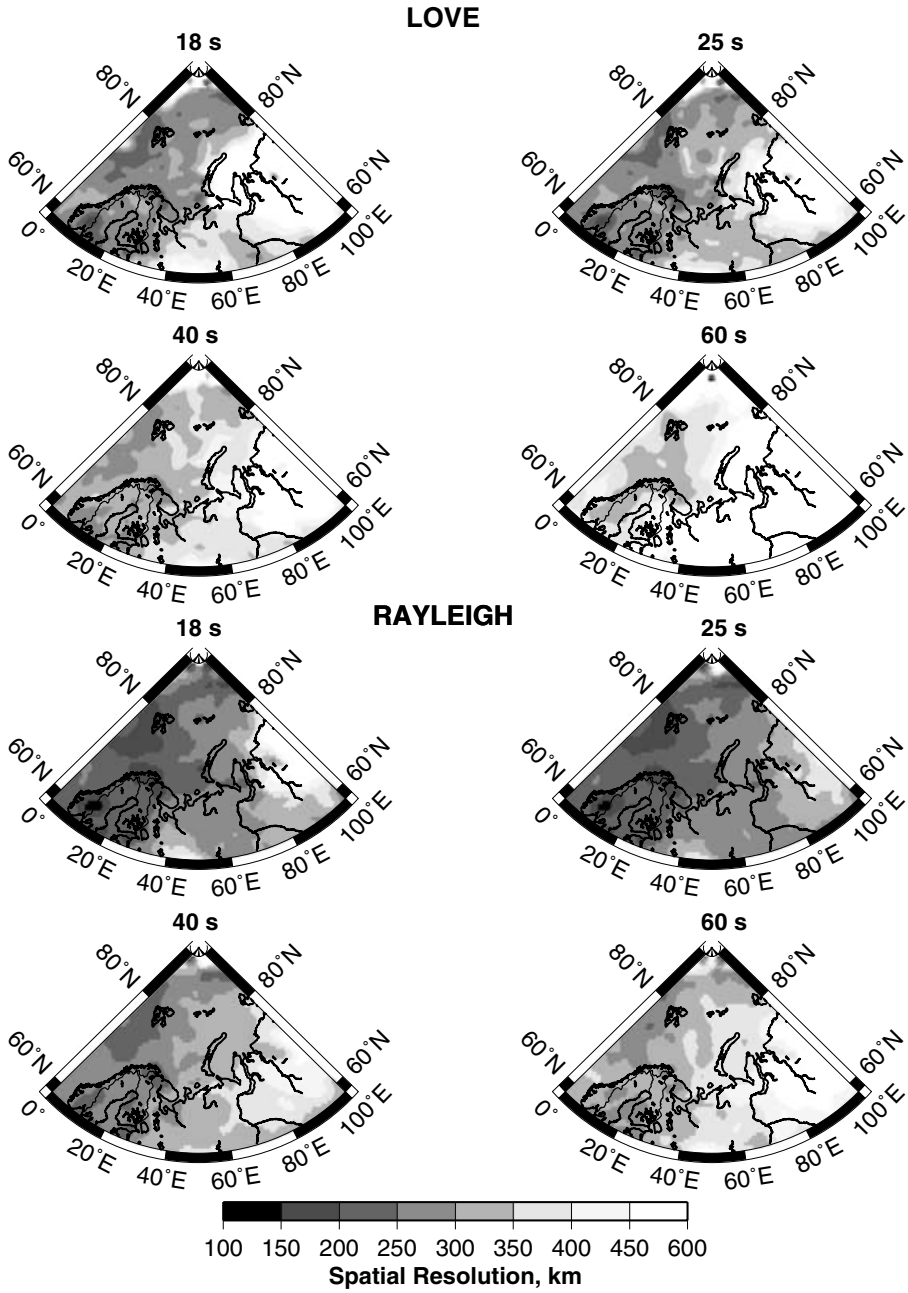

Figure 9. Resolution maps for Love (top) and Rayleigh (bottom) waves for different investigated periods.

data centres IRIS and GEOFON. We gratefully acknowledge the data made available by these organizations.

We thank Hilmar Bungum for initiating the cooperation of NORSAR and CU-Boulder, Nils Maercklin for providing us with a resampled version of the crustal model BARENTS50, Michail Barmin for creating a transportable version of CU software, and Jan Inge Faleide for important comments on geotectonical aspects of this work. A. Levshin is very grateful to the administrations of the NORSAR and the Department of Geosciences, University of Oslo, for the opportunity to work for three months at NORSAR. Ch. Weidle was partly funded by a postdoctoral scholarship of the Norwegian Research Council. We thank the Editor Tim Minshull, Walter Mooney and an anonymous reviewer for thoughtful and constructive reviews. Most figures have been plotted using GMT (Wessel & Smith 1995).

This is NORSAR contribution 972.

REFERENCES

Antolik, M., Gu, Y.J., Dziewonski, A.M. & Ekström, G., 2003. A new joint model of compressional and shear velocity in the mantle, *Geophys. J. Int.,* **153,** 443–466.

Artyushkov, E.V., 2004. Mechanism of the formation of deep sedimentary basins on continents: The Barents Basin, *Doklady RAN, Earth Sciences,* **397**(5), 595–599.

Artyushkov, E.V., 2005. The formation mechanism of the Barents basin *Russian Geology and Geophysics,* **46**(7), 683–696.

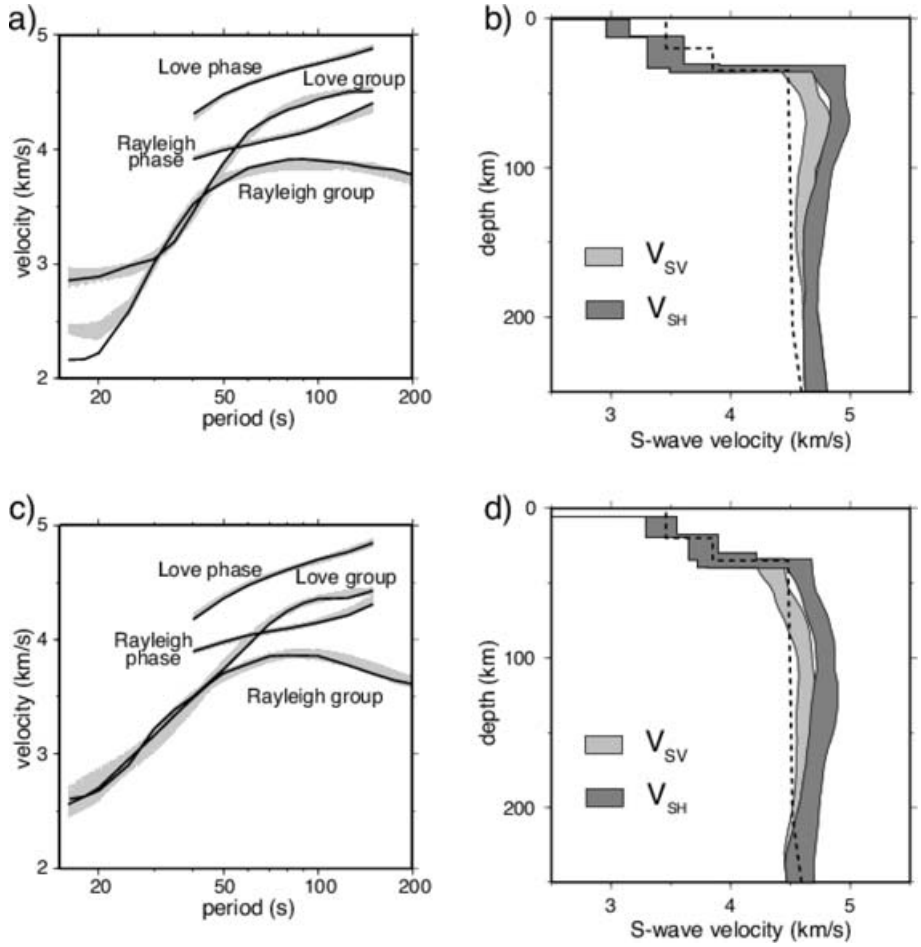

Figure 10. Examples of the inversion for acceptable 1-D shear velocity models. (a) and (b) A point in the Barents Sea (74°N, 40°E). (c) and (d) A point in Western Siberia (70°N, 70°E). (a) and (c) Four dispersion curves obtained from tomographic velocity maps (thick black lines) and the predictions from the ensemble of acceptable models (grey lines) shown in (b) and (d), respectively. (b) and (d) The ensemble of acceptable models where SV and SH velocities are presented with light and dark grey shades, respectively. The corridor of acceptable values is indicated by the solid black lines. The *S*-wave velocity from the global reference model ak135 (Kennett *et al.* 1995) is plotted as the dash line.

Barmin, M.P., Ritzwoller, M.H. & Levshin, A.L., 2001. A fast and reliable method for surface wave tomography, *Pure appl. Geophys.,* **158,** 1351–1375.

Bassin, C., Laske, G. & Masters, G., 2000. The current limits of resolution for surface wave tomography in North America, *EOS, Trans. Am. geophys. Un.,* **81**(48), F879, Abstract S12A-03.

Breivik, A.J., Verhoef, J. & Faleide, J.I., 1999. Effect of thermal contrasts on gravity modeling at passive margins: Results from the western Barents Sea, *J. geophys. Res.,* **104,** 15 293–15 311.

Breivik, A.J., Mjelde, R., Grogan, P., Shimamura, H., Murai, Y., Nishimura, Y. & Kuwano, A., 2002. A possible Caledonide arm through the Barents Sea imaged by OBS data, *Tectonophysics,* **355,** 67–97.

Bungum, H. & Capon, J., 1974. Coda pattern and multipath propagation of Rayleigh waves at NORSAR, *Phys. Earth planet. Int.,* **9,** 111–127.

Bungum, H., Ritzmann, O., Maercklin, N., Faleide, J.I., Mooney, W.D. & Detweiler, S.T., 2005. Three-dimensional model for the crust and upper mantle in the Barents Sea region, *EOS, Trans. Am. geophys. Un.,* **86,** 160–161.

Calcagnile, G. & Panza, G.F., 1978. Crust and upper mantle structure under the Baltic shield and Barents Sea from the dispersion of Rayleigh waves, *Tectonophysics,* **47,** 59–71.

Chan, W.W. & Mitchell, B.J., 1985. Surface wave dispersion, crustal structure and sediment thickness variations across the Barents shelf, *Geophys. J. R. astr. Soc.,* **68,** 329–344.

Dimakis, P., Braathen, B.I., Faleide, J.I., Elverhøi, A. & Gudlaugsson, S.T., 1998. Cenozoic erosion and the preglacial uplift of the Svalbard-Barents Sea region. *Tectonophysics,* **300,** 311–327.

Ebbing, J., Braitenberg, C. & Skilbrei, J.R., 2005. Basement characterisation by regional isostatic methods in the Barents Sea. *NGU Report 2005.074,* p. 78.

Egorkin, A.A., Levshin, A.L. & Yakobson, A.N., 1988. Study of the deep structure of the Barents Sea shelf by seismic surface waves, in *Numerical modeling and analysis of geophysical processes, Computational Seismology,* Vol. 20, pp. 197–201, ed. Keilis-Borok, V.I., Allerton Press, NY.

Ekström, G., Tromp, J. & Larson, E.W.F., 1997. Measurements and global models of surface wave propagation, *J. geophys. Res.,* **102,** 8137–8157.

Engdahl, E.R. & Schweitzer, J., 2004a. Observed and predicted travel times of Pn and P phases recorded at NORSAR from regional events, *Semiannual Technical Summary, 1 January–30 June 2004, NORSAR Scientific Report,*2-2004, 51–56.

Engdahl, E.R. & Schweitzer, J., 2004b. Observed and predicted travel times of Pn and P phases recorded at NORSAR from regional event, *EOS, Trans. Am. geophys. Un.,* **85**(47), Abstract S13B-1050.

Faleide, J.I., Ritzmann, O., Weidle, C. & Levshin, A., 2006a. Geodynamical aspects of a new 3-D geophysical model of the greater Barents Sea region—linking sedimentary basins to the upper mantle structure, *Geophys. Res. Abstr.,* **8,** 08640.

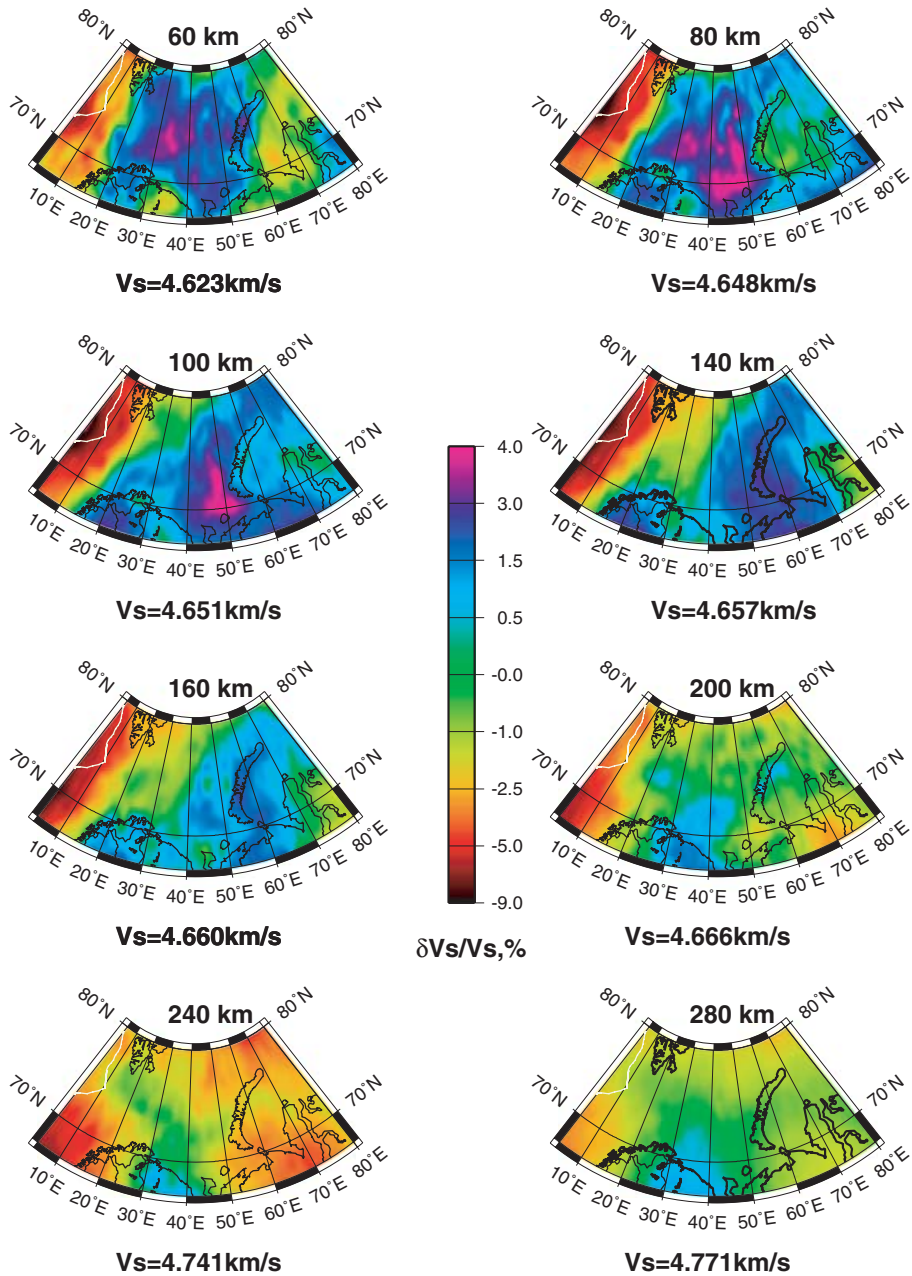

Figure 11. Results of the 3-D tomographic inversion: isotropic shear wave velocities $V_s = (V_{sv} + V_{sh})/2$ at different depths relative to the 1-D model *Barey*. The reference *S*-velocities are presented below each map.

Faleide, J.I., Ritzmann, O., Weidle, C., Levshin, A. & Gee, D., 2006b. Linking Eastern Barents Sea basin formation to the deep crustal and upper mantle structure. *AGU Fall Meeting 2006, abstract*.

Goes, S., Govers, R. & Vacher, R., 2000. Shallow mantle temperatures under Europe from P and S wave tomography, *J. geophys. Res.,* **105,** 11 153–11 169.

Gudlaugsson, S.T., Faleide, J.I., Johansen, S.E. & Breivik, A.J., 1998. Late Palaeozoic structural development of the South-western Barents Sea, *Mar. Petrol. Geol.,* **15,** 73–102.

Hicks, E.C., Kværna, T., Mykkeltveit, S., Schweitzer, J. & Ringdal, F., 2004. Travel times and attenuation relations for regional phases in the Barents Sea region, *Pure appl. geophys.,* **161,** 1–19.

Johansen, S.E. *et al.*, 1992. Hydrocarbon potential in the Barents Sea region: play distribution and potential, in *Arctic geology and petroleum potential, NPF Special Publication 2,* pp. 273–320. eds Vorren, T.O., Bergsaker, E., Dahl-Stamnes, Ø.A., Holter, E., Johansen, B., Lie, E. & Lund, T.N., Elsevier, Amsterdam.

Kennett, B.L.N., Engdahl, E.R. & Buland R., 1995. Constraints on seismic velocities in the Earth from traveltimes, *Geophys. J. Int.,* **122,** 108–124.

Kremenetskaya, E., Asming, V. & Ringdal, F., 2001. Seismic location calibration of the European Arctic, *Pure appl. geophys.,* **158,** 117–128.

Levshin, A. & Berteussen, K.-A., 1979. Anomalous propagation of surface waves in the Barents Sea as inferred from NORSAR recordings, *Geohys. J. R. astr. Soc.,* **56,** 97–118.

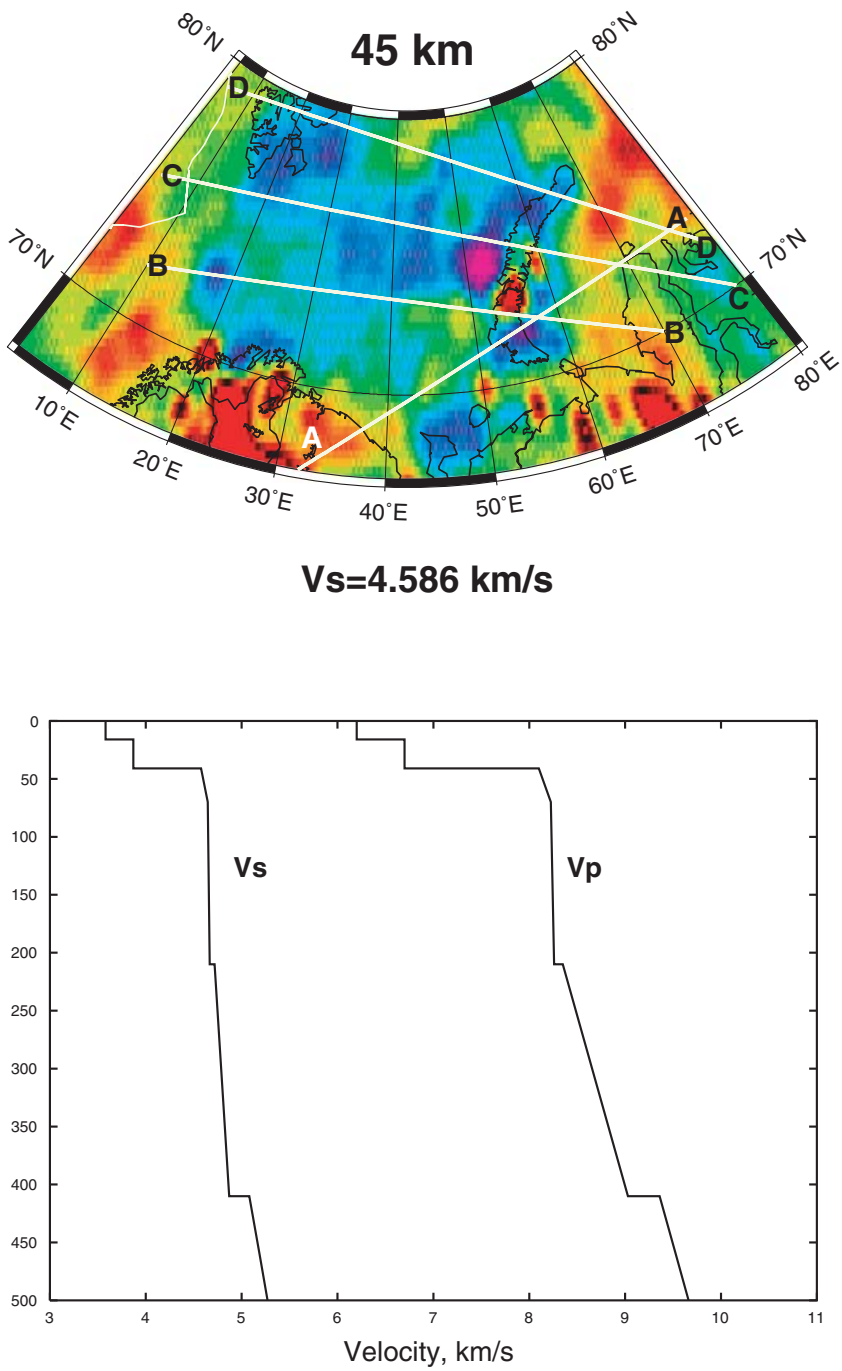

Figure 12. Results of the 3-D tomographic inversion: isotropic shear wave velocities $V_s = (V_{sv} + V_{sh})/2$ at 45 km relative to the 1-D model *Barey* (top). The map contains in addition the position of the different transects through the model as shown in Fig. 13. The *Barey* model (Schweitzer & Kennett 2002) used in this study as 1-D reference model is shown at the bottom.

Levshin, A., Weidle, Ch. & Schweitzer, J., 2005a. Surface wave tomography for the Barents Sea and surrounding regions, *Semiannual Technical Summary, 1 January–30 June 2005, NORSAR Scientific Report,*2-2005, 37–48.

Levshin, A., Schweitzer, J., Weidle, Ch., Maercklin, N., Shapiro, N. & Ritzwoller, M., 2005b. Surface wave tomography of the European Artic, *EOS, Trans. Am. geophys. Un.,* **86**(52), Fall Meeting Supplement, Abstract S51E-1053.

Levshin, A.L., Ritzwoller, M.H., Barmin, M.P., Villaseñor, A. & Padgett, C.A., 2001. New constraints on the Arctic crust and uppermost mantle: surface wave group velocities, Pn, and Sn, *Phys. Earth planet. Int.,* **123,** 185–204.

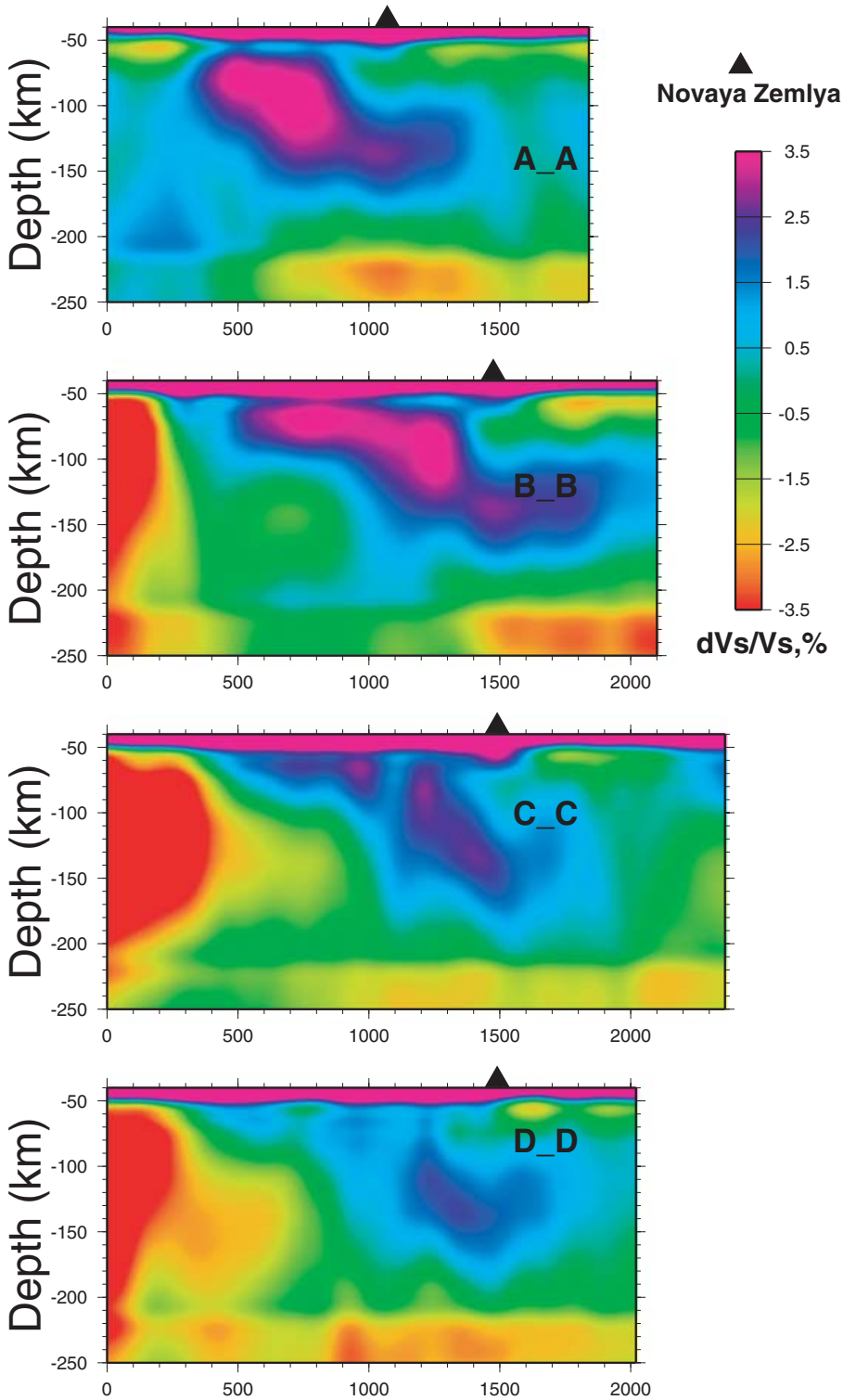

Figure 13. Isotropic *S*-velocity ($V_s = (V_{sv} + V_{sh})/2$) perturbations relative to the *Barey* model along four transects shown in Fig. 12.

Mann, P., Gahagan, L. & Gordon, M.B., 2004. Tectonic setting of the world's giant oil and gas fields, in *Giant oil and gas fields of the decade 1990–1999,* pp. 15–105, ed. Halbouty, M.T., AAPG Memoir 78.

McCowan, D.W., Glover, P. & Alexander, S.S., 1978. A crust and upper mantle model for Novaya Zamlya from Rayleigh wave dispersion data, *Bull. seism. Soc. Am.,* **68,** 1651–1662.

Pasyanos, M.E., 2005. A variable resolution surface wave dispersion study of Eurasia, North Africa, and surrounding regions, *J. geophys. Res.,* **110,** B12301, doi:10.1029/2005JB003749, 22 pp.

Ritzmann, O., Maercklin, N., Faleide, J.I., Bungum, H., Mooney, W.D. & Detweiler, S.T., 2007. A three-dimensional geophysical model for the crust in the Barents Sea region: model construction and basement

characterisation, *Geophys. J. Int.,* doi: 10.1111/j.1365-246X.2007.03337.x.

NOAA, 1988. Data Announcement 88-MGG-02, Digital relief of the Surface of the Earth, National Geophysical Data Center, Boulder, Colorado.

Ritzwoller, M.H. & Levshin, A.L., 1998. Eurasian surface wave tomography: Group velocities, *J. geophys. Res.,* **103,** 4839–4878.

Ritzwoller, M.H., Shapiro, N.M., Barmin, M.P. & Levshin, A.L., 2002. Global surface wave diffraction tomography, *J. geophys. Res.,* **107**(B12), 2335, ESE 4–1 – 4–13, doi:10.1029/2002JB001777.

Ritzwoller, M.H., Shapiro, N.M., Levshin, A.L., Bergman, E.A. & Engdahl, E.R., 2003. The ability of a global 3-D model to locate regional events, *J. geophys. Res.,* **108**(B7), 2353, ESE 9-1–9-24.

Schweitzer, J., 1999. The MASI–1999 field experiment, *Semiannual Technical Summary, 1 April–30 September 1999, NORSAR Scientific Report,* 1-1999/2000, 91–101.

Schweitzer, J. & Kennett, B.L.N., 2002. Comparison of location procedures—the Kara Sea event of 16 August 1997, *Semiannual Technical Summary, 1 July 2001–31 December 2001, NORSAR Scientific Report,* 1-2002, 97–114.

Shapiro, N.M. & Ritzwoller, M.H., 2002. Monte-Carlo inversion for a global shear velocity model of the crust and upper mantle, *Geophys. J. Int.,* **151,** 88–105.

Shapiro, N.M. & Ritzwoller, M.H., 2004. Thermodynamic constraints on seismic inversions, *Geophys. J. Int.,* **157,** 1175–1188, doi:10.1111/j.l365–246X.2004.02254.x.

Trampert, J. & Woodhouse, J.H., 1995. Global phase velocity maps of Love and Rayleigh waves between 40 and 150 s period, *Geophys. J. Int.,* **122,** 675–690.

Vorren, T.O., Bergsaker, E., Dahl-Stamnes, Ø.A., Holter, E., Johansen, B., Lie, E. & Lund, T.N., 1990. *Arctic geology and petroleum potential, NPF Special Publication 2*.

Wessel, P.A. & Smith, W.H., 1995. New version of the Generic Mapping Tools released, *EOS, Trans. Am. geophys. Un.,* **76,** Suppl., 329.